JOURNAL OF CATALYSIS 139, 175–190 (1993)

The Effect of Calcination on H_2 Spillover in Pt/MoO_3

II. Kinetic Modelling

J.-G. KIM AND J. R. REGALBUTO[1]

Department of Chemical Engineering, University of Illinois at Chicago, P.O. Box 4348, Chicago, Illinois 60680

Received October 30, 1991; revised June 9, 1992

The effect of catalyst preparation on the the morphology of Pt/MoO_3 and the kinetic effects of hydrogen spillover have been quantitatively investigated in this second of two works. A simplified intrinsic kinetics model of hydrogen spillover has been used to simulate two series of ITR and TPR experiments in Pt/MoO_3 samples. An interpretation of the experimental results consistent with the assumed mechanism is as follows: (1) For the noncalcined or low-temperature (100°C) calcined samples, formation of the hydrogen bronze occurs by a series–parallel mechanism; first, reduction of the MoO_3 surface by hydrogen spillover from Pt must occur, but then direct adsorption of H_2 onto the partially reduced MoO_3 surface supplies most of the hydrogen to the MoO_3 bulk. (2) In the high-temperature calcined samples, hydrogen spillover is effectively the single bronze formation pathway and rate-determining step, as the rate of spillover increases by three orders of magnitude with respect to the noncalcined sample and is much faster than direct adsorption onto the partially reduced MoO_3 surface. (3) In simulations of the high-temperature calcined samples, the activation energy for spillover decreases a small amount, while the preexponential factor increases over 200 times. The most plausible explanation for these trends is thought to be a lessening of blockage of adlineation sites or hindrance of hydrogen diffusion across the Pt surface by residual chlorine.

INTRODUCTION

In the previous study of H_2 spillover in Pt/MoO_3 (*1*), it was shown that an increase in calcination temperature caused the rate of H_2 uptake to increase and the initial temperature of reduction to decrease. Characterization by TEM, chemisorption, and XPS revealed that calcination induced MoO_3 overlayers to grow on Pt, but also showed that the amount of chlorine associated with the Pt phase decreased. It was suggested that the amount of residual chlorine was the predominant cause for the observed trend in H_2 uptake in the series of samples with the same initial Pt precursor dispersion. To further interpret the cause of the increased H_2 uptake rates in these samples, in the present work a simple model of intrinsic kinetics is employed to simulate the isothermal reduction (ITR) and temperature-programmed reduction (TPR) experiments conducted previously.

The integrated kinetics–reactor model is of the type originally developed to model catalytic surface reactions (*2*, *3*) consisting of several simultaneous differential gas and surface mass balances related to the proposed catalytic sequence through the law of mass action for each intrinsic step. An important advantage of this type of model is that a rate-determining step (RDS) need not be assumed, enabling several kinetic regimes to be accounted for with little or no parameter adjustment. The further goal of these types of models is to incorporate to

[1] To whom correspondence should be addressed.

0021-9517/93 $5.00

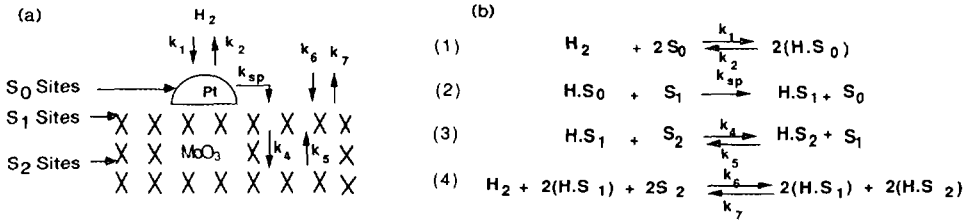

FIG. 1. (a) Schematic diagram of hydrogen spillover model. (b) Elementary steps of H_2 spillover mechanism: (1) H_2 adsorption on Platinum, (2) H_2 spillover step, (3) H_2 diffusion into bulk, (4) H_2 adsorption directly on bronze.

the greatest extent possible independently obtained intrinsic rate constants found from low-pressure or single-crystal studies.

This type of approach has been extended to multicomponent, competitive adsorption (*4*), multisite adsorption (*5*), and absorption or subsurface migration into solids (*5–7*). The framework adopted here to describe hydrogen spillover from Pt crystallites into the bulk of MoO_3 consists of a combination of multisite adsorption (onto Pt and a partially reduced MoO_3 surface) and absorption into the bulk (of MoO_3). The simulation results for spillover in calcined Pt/MoO_3 suggest a change in the RDS changes as the calcination temperature changes and also more clearly suggests how residual chlorine or MoO_3 overlayers affects the hydrogen uptake rate.

THEORY

A schematic of the adsorption–absorption mechanism and the individual reaction steps are shown in Fig. 1. Surface diffusion over both the Pt and MoO_3 phases is assumed to be very rapid, a common assumption of simple lumped parameter models of this type. A rough check of this assumption can be made using the reported values for the bulk diffusion coefficients, 10^{-7}–7.9×10^{-6} cm^2/s (*8*, *9*). The value for the surface area of MoO_3 employed here is 13 m^2/g (*10*), in rough agreement with a limited TEM sampling (7.3 m^2/g) (*1*). From chemisorption data, the average MoO_3 area corresponding to one Pt crystallite is 20,000 nm^2 and the spacing of Pt crystallites is 160 nm. The molar flux of H from diffusion in the bulk, assuming that the concentration gradient is given by the difference of the proton concentration between a full and empty unit cell, divided by the unit cell thickness (*9*) gives a rough value of 1200 $mol/cm^2/s$. Converting this to a linear velocity assuming again the concentration of a full unit cell, results in a velocity of 100 cm/s at the edge of a Pt crystallite, which reduces to a value of about 5 cm/s midway between Pt particles. Mixing is established in microseconds, using the bulk diffusion coefficient. Even if the surface diffusion coefficient is many orders of magnitude larger than the bulk diffusion coefficient, good mixing still seems plausible since the duration of kinetic effects seen in the ITR and TPR experiments is on the order of tens of minutes.

Values for intrinsic, fixed rate constants and their references are given in Table 1. Hydrogen adsorption is modeled to occur dissociatively over Pt (step 1), as is commonly reported (*11–13*, *15*). The number of Pt sites (S_{0T}) in each experiment was determined by selective chemisorption (*1*), and is presented with other calculated parameters (S_{1T} and S_{2T}) in Table 2. The number of Pt exposed sites for the highest calcination temperature drops to 14% of the noncalcined sample due to Pt coverage by overlayers of MoO_3 (*1*). The H_2 adsorption rate constant was calculated from kinetic theory, and the sticking coefficient of 0.1 (*8*) was used. The desorption preexponential factor

TABLE 1

Values of Parameter for Spillover Model

Symbol	Meaning	Units	Value	Source
k_{col1} (Pt)	Collision rate constant	s^{-1}	$1.48 \times 10^{12} (273 + T)^{0.5}$	Theory (*7*)
Sc_1 (Pt)	Sticking coefficient	none	0.099	(*11*)
k_{col6} (MoO_3)	Collision rate constant	s^{-1}	$2.43 \times 10^{10} (273 + T)^{0.5}$	Theory (*7*)
Sc_6 (MoO_3)	Sticking coefficient	none	10^{-7}	This work
S_{0T}	Total surface moles of Pt	mol	Table 2	Measured
S_{1T}	Total surface moles of MoO_3	mol	Table 2	(*10*)
S_{2T}	Total bulk moles of MoO_3	mol	Table 2	Calculated
k_{20}	Preexp'l, desorption	$mol^{-1}\ s^{-1}$	10^{13}	(*12*)
E_2	Desorption act. energy	cal/mol	1.75×10^4	
k_{sp}	Preexp'l, spillover	$mol^{-1}\ s^{-1}$	Table 3	This work
E_{sp} for ITR	Spillover act. energy in ITR	cal/mol	1.15×10^4	(*19*)
E_{sp} for TPR	Spillover act. energy in TPR	cal/mol	Table 3	This work
k_{40}	Preexp'l, penetration	$mol^{-1}\ s^{-1}$	$4.7 \times 10^7\ k_{sp0} \exp(E_{sp}/E_4)$	(*8*)
E_4	Penetration act. energy	cal/mol	0.94×10^4	(*14*)
k_{50}	Preexp'l, back diffusion	$mol^{-1}\ s^{-1}$	9.15×10^{18}	This work
E_5	Back diffusion act. energy	cal/mol	0.94×10^4	(*14*)

and desorption activation energy were taken from the work of Seebauer *et al.* (*11*) and Zhdanov (*12*), respectively.

It was found necessary to include a term for dissociative adsorption of H_2 directly onto the partially reduced MoO_3 surface (step 4 of Fig. 1b), a phenomenon reported by Fripiat and co-workers over single-crystal MoO_3 (the 100 face) at low pressure (*9*, *16*). Step 4 is similar to the form originally postulated (*16*),

$$H_2 + 2S_{ox} \leftrightarrow 2S_{red}H,$$

except that as written above dissociative adsorption would occur over the unreduced trioxide, which does not physically occur. Partially reduced MoO_3 sites are necessary, and the inclusion of two such sites on either side of step 4 represents the catalytic role of these sites for the dissociative adsorption of hydrogen. The value for rate constant for this reaction was obtained from the experimental data, as described in the results, and is reported as the adsorption rate constant from kinetic theory multiplied by the fitted sticking coefficient (Table 1). The collision frequency for MoO_3 differs from that of Pt due to different surface densities of the two materials.

TABLE 2

Values of S_{0T}, S_{1T}, and S_{2T} (mol)

ITR	$S_{0T} \times 10^6$	$S_{1T} \times 10^5$	$S_{2T} \times 10^3$	
			ITR	TPR
Noncalcined	0.952	3.796	1.835	2.446
100°C Calcined	0.889	3.802	2.140	2.446
200°C Calcined	1.013	3.790	2.446	2.344
300°C Calcined	0.903	3.801	2.956	2.344
400°C Calcined	0.398	3.852	2.772	2.344
500°C Calcined	0.129	3.879	2.201	2.344

The number of MoO_3 surface sites (S_{1T}) was calculated from the surface area of the MoO_3 samples and is given in Table 2. Adsorption onto MoO_3 was assumed irreversible ($k_7 = 0$). The value for the forward penetration rate constant (k_4) was constrained by results of Taylor *et al.* (*8*) that the rate constant of H penetration into bulk MoO3 was 4.7×10^7 times faster than the spillover rate constant. This relationship was kept constant with changing temperatures by using the relation shown in Table 1 along with the k_{sp} and E_{sp} values for the noncalcined sample. The value for the back

penetration rate constant (k_5) was adjusted (as described in the results) to values much lower than the forward penetration rate constant, consistent with reports that the MoO_3 surface is self-cleaning (*16*).

The number of bulk MoO_3 sites (S_{2T}) was taken from the integrated H_2 uptake area of each sample used in the ITR or TPR runs; these are also given in Table 2. A more rigorous manner of varying S_{2T} between the ITR and TPR runs would be to keep the total number of bulk number of sites constant, but vary the forward and reverse diffusion constants to reflect the thermodynamically dictated lower bronze composition at the higher temperature of the TPR experiment. This method, however, could not accurately reflect the number of MoO_3 particles isolated by extensive overlayer formation at the higher calcination temperatures, without an additional adjustment. The number of S_1 and S_2 sites is approximately constant in the series of samples; the only major difference between samples is the number of exposed Pt sites.

The hydrogen spillover step (step 2) is modelled as the product of a rate constant, Pt surface coverage by hydrogen, and the fraction of open MoO_3 surface sites,

$$r_{\text{spillover}} = k'_{\text{sp}}\text{H} \cdot S_0 S_1$$

or

$$r_{\text{spillover}} = k'_{\text{sp}} S_{0T} S_{1T} \theta_{S_0}(1 - \theta_{S_1})$$

in scaled form and including surface mole balances. A more rigorous spillover model would have the true intrinsic spillover rate constant multiplied by the number of adlineation sites,

$$r_{\text{spillover}} = k'_{\text{sp}} S_{01} \theta_{S_0}(1 - \theta_{S_1})$$

where S_{01} represents the number of adlineation sites and is some function of S_0 and S_1. In a series of samples in which no overlayers were present, and Pt existed as Pt^0, S_{01} would simply be the number of Pt perimeter sites and could be calculated directly from chemisorption data. The diameter of Pt particles has, in fact, been estimated from measured spillover rate constants in this vein (*17*). However, in the presence of MoO_3 overlayers on Pt, or when residual chlorine potentially blocks adlineation sites, the calculation based on Pt perimeter is not valid. Consequently, the number of adlineation sites will be lumped into the spillover rate constant, that is, $k_{\text{sp}} = k'_{\text{sp}} S_{01}$. The strategy for determining values of k_{sp} will be described in the results, and the implications of this lumping of the fraction of adlineation sites into k_{sp} will be discussed.

The intrinsic kinetic model consists of four transient mass balances: one for the reactor gas phase, and one each for H adsorbed on Pt ($\text{H} \cdot S_0$), H on the surface of MoO_3 ($\text{H} \cdot S_1$), and H in the bulk of MoO_3 ($\text{H} \cdot S_2$). The accumulation of hydrogen in the gas phase includes the reactor balance and the net loss or gain from the Pt and MoO_3 surfaces:

$$V\frac{d\text{H}_2}{dt} = Q(\text{H}_{2\text{in}} - \text{H}_2) - (k_1 H_2 S_0^2 - k_2(\text{H} \cdot S_0)^2) - (k_6 \text{H}_2(\text{H} \cdot S_1)^2(S_2)^2 - k_7(\text{H} \cdot S_1)^2(\text{H} \cdot S_2)^2). \quad (1)$$

Hydrogen accumulation on the Pt surface, $\text{H} \cdot S_0$, equals the adsorption minus the desorption rate, minus the loss due to spillover:

$$\frac{d\text{H} \cdot S_0}{dt} = k_1 \text{H}_2 S_0^2 - k_2(\text{H} \cdot S_0)^2 - k_{\text{sp}}(\text{H} \cdot S_0)S_1. \quad (2)$$

Hydrogen accumulation on the MoO_3 surface, $\text{H} \cdot S_1$, equals the gain from spillover, less the net diffusion rate into the bulk, plus the net H_2 adsorption rate directly onto MoO_3:

$$\frac{d\text{H} \cdot S_1}{dt} = k_{\text{sp}}(\text{H} \cdot S_0)S_1 - k_4(\text{H} \cdot S_1)S_2 + k_5(\text{H} \cdot S_2)S_1 + k_6 \text{H}_2(\text{H} \cdot S_1)^2 S_2^2 - k_7(\text{H} \cdot S_1)^2(\text{H} \cdot S_2)^2. \quad (3)$$

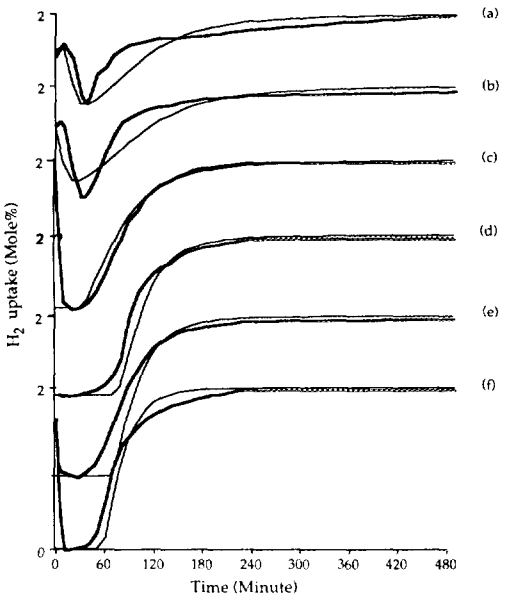

FIG. 2. H_2 uptake in ITR at 50°C, experiment (▬▬) vs model (———): (a) noncalcined; calcinations at (b) 100°C, 1 h; (c) 200°C, 1 h; (d) 300°C, 1 h, (e) 400°C, 1 h; (f) 500°C, 1 h.

The accumulation of H in bulk MoO_3 is given as the sum of the net rates of diffusion from the surface layer and direct H_2 adsorption onto the MoO_3 surface:

$$\frac{d\mathrm{H}\cdot S_2}{dt} = k_4(\mathrm{H}\cdot S_1)S_2 - k_5(\mathrm{H}\cdot S_2)S_1 + k_6\mathrm{H}_2(\mathrm{H}\cdot S_1)^2S_2^2 - k_7(\mathrm{H}\cdot S_1)^2(\mathrm{H}\cdot S_2)^2. \quad (4)$$

Surface and bulk mass balances are

$$S_{i\mathrm{T}} = S_i + \mathrm{H}\cdot S_i \quad \text{or} \quad S_i = S_{i\mathrm{T}} - \mathrm{H}\cdot S_i,$$

where $i = 0$, 1, or 2 for the Pt surface, MoO_3 surface, or MoO_3 bulk, respectively. These are substituted into Eqs. (1)–(4). The equations are then scaled by the inlet hydrogen concentration, $S_{0\mathrm{T}}$, $S_{1\mathrm{T}}$, or $S_{2\mathrm{T}}$ where appropriate, and are solved with a standard differential equation solving package.

RESULTS

The ITR and TPR runs which were simulated are shown in Figs. 2 and 3, respectively. The simulations shown represent the best fits of all adjustable parameters; in each of the sensitivity analyses to follow (Figs. 4–7), one particular rate parameter will be perturbed about this best fit (BF) value. Sensitivity analyses were performed with simulations of the noncalcined sample, which represents the highest amount of exposed Pt surface area in the series, and the 500°C calcined sample, which represents the lowest amount of exposed Pt area. The process with which the final set of parameters was derived and from which mechanistic interpretations are made are now discussed.

The initial attempt of the modelling effort was to determine if all ITR and TPR experiments could be adequately simulated by fitting only the spillover rate constant, k_{sp},

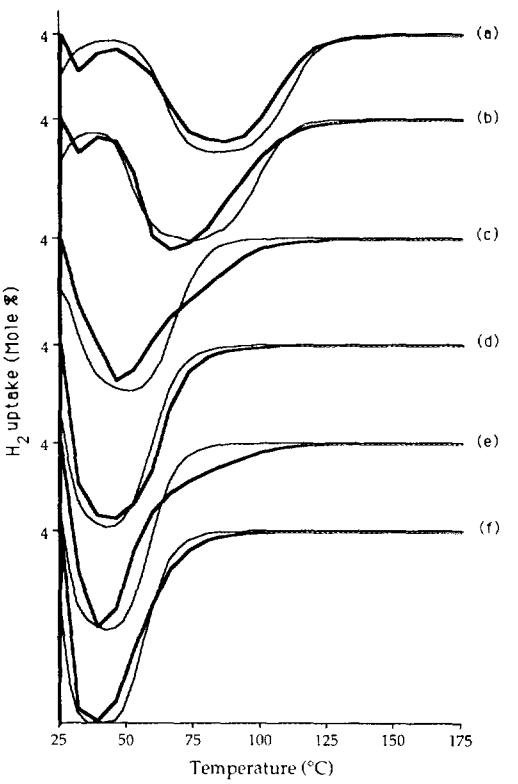

FIG. 3. H_2 uptake in TPR, experiment (▬▬) vs model (———): (a) noncalcined; calcinations at (b) 100°C, 1 h; (c) 200°C, 1 h; (d) 300°C, 1 h, (e) 400°C, 1 h; (f) 500°C, 1 h.

while neglecting entirely mechanistic step 4, H_2 adsorption onto partially reduced MoO_3. These initial simulation runs failed to reproduce the lag time and initial maximum seen in the noncalcined and 100°C calcined samples of both sets of experiments (Figs. 2 and 3, spectra a and b). The lag time and inflection point could be reproduced only with a combination of spillover and direct H_2 adsorption onto the bronze.

Incorporating the mechanism of H_2 adsorption onto the partially reduced MoO_3 surface required two additional adjustable parameters, one the rate constant for adsorption onto the S_1 surface, k_6, and the other the value of the bulk back penetration rate constant k_5. The latter rate constant had to be made smaller than the bulk forward rate constant (k_4), so that the adsorption capacity of the MoO3 surface was regenerated, yet not so small that sufficient $H \cdot S_1$ could not accumulate for step 4 to proceed. Once values for k_6 and k_5 were established for simulations of the noncalcined samples, they were kept constant since there is no physical reason why they should change. That is, the MoO_3 surface is assumed to be largely unaffected by different temperature treatments in oxygen. Orthorhombic MoO3 is known to form irreversibly from the ammonium hyeptamolybdate precursor, and has been shown to be completely stable to additional calcinations at 300°C (*18*). With these two values established, it was possible to simulate the rest of the ITR spillover runs (Fig. 2) satisfactorily by changing only the spillover rate constant. This "bootstrapping" procedure for finding the best values of rate constants, possible due to the nature of this transient kinetic model, reduces the number of adjustable parameters for any one set of experiments and also simplifies the optimization routine. If a sufficient range of experimental conditions is simulated, the rate parameters can be optimized one (or a few) at a time.

The sensitivity of the simulations of the noncalcined samples to the three rate constants k_{sp}, k_6, and k_5, can be seen in Fig. 4, 5, and 6. The sensitivity of the H_2 uptake spectra for the noncalcined sample to k_{sp} is shown in Fig. 4a, and for the 500°C calcined sample, in Fig. 4b. In Fig. 4a, the lowest spillover rate resulted in the longest lag time. Increasing k_{sp} by a factor of 10 and 200 only decreased the lag time but did not significantly change the shape of the reduction profile. The shape of the reduction profile at these lower spillover rates can be altered only by changing the value of k_6 (Fig. 5). The interpretation is as follows: for the noncalcined or 100°C calcined samples the spillover rate controls the rate of reduction of the MoO_3 surface, but once the surface is sufficiently reduced, reduction of the bulk occurs primarily by H_2 adsorption onto the MoO_3 surface.

For the 500°C calcined sample, Fig. 4b, a much larger value of k_{sp} is needed to model the data. The simulation is still sensitive to changes in k_{sp} and is more sensitive to decreases than to increases. Insensitivity at the highest values of the spillover rate must mean that spillover is no longer rate determining, but that H_2 adsorption is. This condition is far removed from the simulated experiment, however. The same trends were noted for the noncalcined and 500°C calcined simulations of the TPR experiments.

The sensitivity of the ITR simulation for the noncalcined sample to k_6 is shown in Fig. 5a. With no adsorption onto the MoO_3 surface, the reduction occurs at an almost negligible pace. Increasing k_6 deepens the reduction profile but does not change the lag time except at the highest values of k_6. The reason is that for the same spillover rate, the MoO_3 surface becomes reduced at the same time in all the curves. At the highest values of k_6 the bulk reduction can occur with a much lesser extent of reduction of the MoO_3 surface. This does not appear to occur in the realm of the experiment, however. The same qualitative arguments can be made for the effect of k_6 on the TPR simulations, seen in Fig. 5b.

In simulations of the 500°C calcined samples (Fig. 5c for ITR and Fig. 5d for TPR)

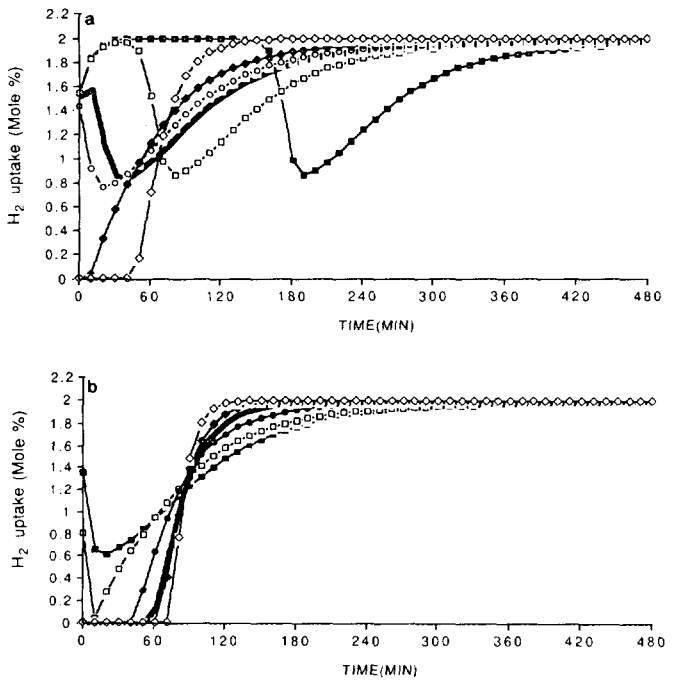

FIG. 4. (a) Effect of variation of spillover rate (k_{sp}) on ITR model for noncalcined 1% Pt/MoO_3, k_{sp} (mol^{-1} s^{-1}) of: —■— 1.65×10^1; —□— 1.65×10^2; ▬▬ 3.31×10^3 (BF); —○— 1.65×10^4; —◆— 1.65×10^5; —◇— 1.65×10^6. (b) 500°C Calcined 1% Pt/MoO_3, k_{sp} (mol^{-1} s^{-1}) of: —■— 1.65×10^5; —□— 8.26×10^5; —●— 4.13×10^6; ▬▬ 9.92×10^6 (BF); —◆— 1.49×10^7; —◇— 4.96×10^7.

higher values of k_{sp} are employed. These profiles are almost completely independent of the value of k_6. In Fig. 5c, the value of k_6 has to be increased three orders of magnitude above the highest value used in Fig. 5a for any appreciable effect to be seen. The reason for this insensitivity is that the rate of bulk reduction by spillover is very much larger than the rate of bulk reduction by adsorption onto the MoO_3 surface.

Figure 6a shows the effect of perturbing k_5 about the best fit value for the noncalcined sample simulation. Increasing the value of k_5 causes a more rapid reduction, while decreasing k_5 lowers the rate. The best fit value for the backward penetration value, 4×10^{-12} (mol^{-1} s^{-1}) at 50°C, is much smaller than the forward penetration constant, 1.1×10^{-23} (mol^{-1} s^{-1}). Interestingly, for the 500°C calcined simulation, Fig. 6b, the effect is the opposite. Increasing the value of k_5 from the best fit value lowers the rate of reduction, while decreasing k_5 increases the rate of reduction slightly. The difference between the two cases is that the spillover rate is much larger in the latter case; the corresponding interpretation is that when spillover is slow, increases in the level of S_1 surface coverage bring about faster adsorption onto the bronze, while if the spillover rate is fast, increasing the level of $H \cdot S_1$ slows down the spillover rate which is proportional to the fraction of open S_1 sites. The same trends are noted for TPR sensitivity analyses for the noncalcined and 500°C calcined simulations.

The general indication with the assumed mechanism is that at higher calcination temperatures, spillover is much faster than adsorption onto the bronze and is the only rate

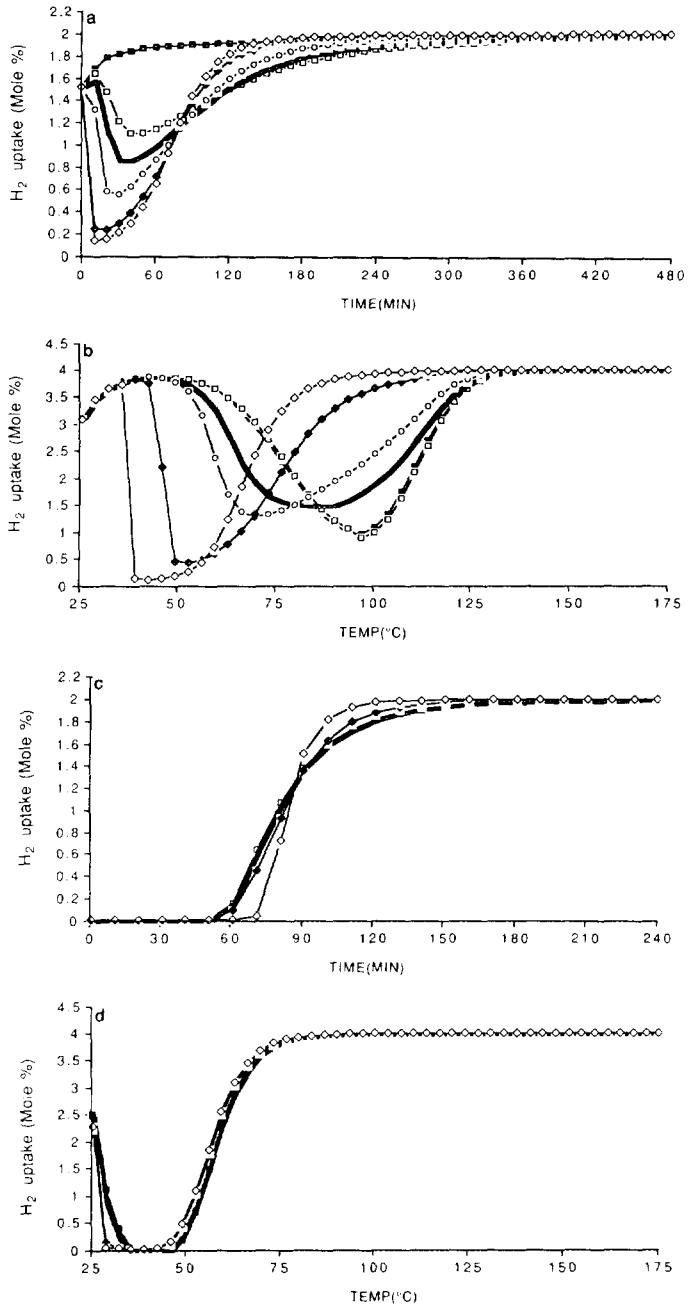

FIG. 5. (a) Effect of variation of H_2 adsorption rate on bronze (k_6) on ITR model for noncalcined 1% Pt/MoO_3, k_6 (s^{-1}) of: —■— none; —□— 2.62×10^4; ▬▬ 4.36×10^4 (BF); —○— 8.73×10^4; —◆— 2.62×10^5; —◇— 4.36×10^5. (b) Noncalcined 1% Pt/MoO_3, K_6 (s^{-1}, at 50°C/175°C) of: —■— none; —□— $8.73 \times 10^1/1.03 \times 10^2$; ▬▬ 4.36×10^4 (BF)/5.14×10^4 (BF); —○— $8.79 \times 10^4/1.03 \times 10^5$; —◆— $4.36 \times 10^5/5.14 \times 10^5$; —◇— $1.54 \times 10^6/2.06 \times 10^6$. (c) 500°C Calcined 1% Pt/MoO_3, k_6 (s^{-1}) of: —■— none; —□— 8.73×10^2; ▬▬ 4.36×10^4 (BF); —○— 8.73×10^5; —◆— 8.73×10^6; —◇— 8.73×10^7. (d) 500°C Calcined 1% Pt/MoO_3, k_6 (s^{-1}, at 50°C/175°C) of: —■— none; —□— $8.73 \times 10^1/1.03 \times 10^2$; —●— $8.73 \times 10^2/1.03 \times 10^3$; ▬▬ 4.36×10^4 (BF)/5.14×10^4 (BF); —◆— $3.49 \times 10^5/4.11 \times 10^5$; —◇— $8.73 \times 10^5/1.03 \times 10^6$.

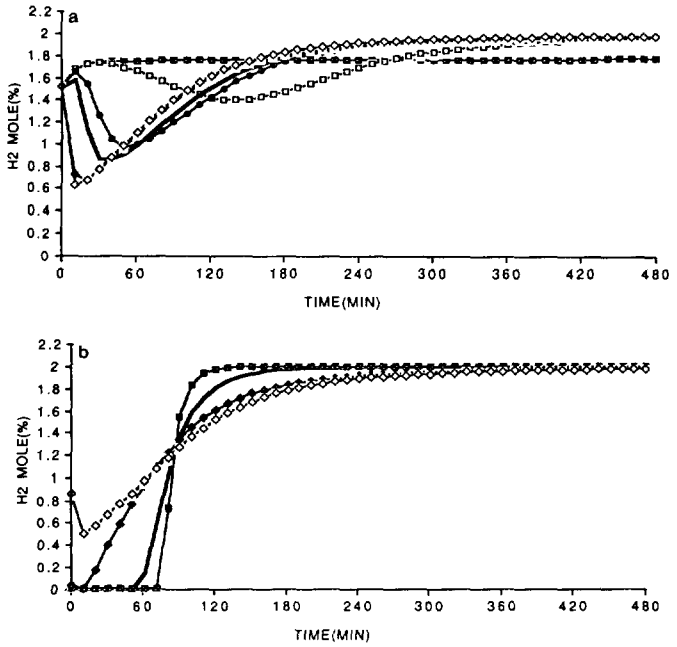

FIG. 6. (a) Effect of variation of diffusion rate (k_5) on ITR model for noncalcined 1% Pt/MoO_3, k_6 ($mol^{-1}\ s^{-1}$) of: —■— 3.99×10^9; —□— 3.99×10^{11}; —●— 2.00×10^{12}; ▬▬ 3.99×10^{12} (BF); —◆— 3.99×10^{13}; —◇— 3.99×10^{15}. (b) 500°C Calcined 1% Pt/MoO_3, k_6 ($mol^{-1}\ s^{-1}$) of: —■— 7.98×10^9; —□— 3.99×10^{10}; —●— 3.99×10^{11}; ▬▬ 3.99×10^{12} (BF); —◆— 3.99×10^{13}; —◇— 3.99×10^{15}.

determining step. For the noncalcined or low-temperature calcined samples the spillover rate is very slow; the predominant bulk reduction pathway is via adsorption onto partially reduced MoO_3. Both steps are necessary, however, as spillover is needed to reduce the MoO_3 surface before direct adsorption can occur. A simplified view of the overall reduction mechanism is as follows:

$$\text{spillover} \rightarrow \begin{array}{c}\text{direct}\\ \text{adsorption}\\ \downarrow\end{array} \begin{array}{l} \\ H \cdot S_1 \\ \\ \end{array} \rightarrow H \cdot S_2.$$

For the noncalcined or low temperature calcined samples, the mechanism shifts from a series to a parallel mechanism, and direct adsorption predominates after the MoO_3 surface becomes partially reduced. For the high-temperature calcined samples, the direct adsorption step is insignificant compared to spillover.

For the noncalcined or 100°C calcined samples, decreases in either rate constant appreciably worsens the fit of the simulation to the experiment, and efforts to increase one to compensate for the decrease in the other do not yield as good a fit. The spillover rate constants used for the simulation curves in Fig. 2 are given in Table 3.

To simulate the TPR experiments (Fig. 3), the spillover rate constant obtained from the

TABLE 3

Values of k_{sp}, k_{spo}, and E_{sp}

Sample	ITR at 50°C k_{sp} ($mol^{-1}\ s^{-1}$)	TPR k_{spo} ($mol^{-1}\ s^{-1}$)	TPR E_{sp} (cal/mol)
Noncalcined	3.31×10^3	3.73×10^{20}	2.52×10^4
100°C Calcined	1.32×10^4	4.29×10^{20}	2.44×10^4
200°C Calcined	3.14×10^5	2.51×10^{21}	2.35×10^4
300°C Calcined	9.83×10^5	7.85×10^{22}	2.35×10^4
400°C Calcined	2.40×10^6	1.91×10^{22}	2.35×10^4
500°C Calcined	9.92×10^6	7.91×10^{22}	2.35×10^4

ITR experiments was used as a constraint, that is, the value for k_{sp} at 50°C was retained. The spillover preexponential factor and activation energy were varied within this constraint to achieve the best fit. All other rate constants were kept the same as for the corresponding ITR simulation; the above overall shift in mechanisms is still found to occur. The sensitivity to changes in preexponential factor and activation energy is shown in Fig. 7. Both Fig. 7a, for the noncalcined sample, and Fig. 7b, for the 500°C calcined sample show that the H_2 uptake profiles are sensitive to changes in k_{spo} and E_{sp}. The preexponential and activation energies of all the simulations in Fig. 3 are listed in Table 3. Of considerable note is that the main effect of calcination was not a lowering of the activation energy, although there was a slight decrease from 25.2 to 23.5 kcal/mol. The preexponential factor increased by a factor of 212 at the highest calcination temperature. This is opposite to the change in the preexponential factor expected of a compensation effect. The spillover rate constant increased by a factor of 3000 at 50°C, or about 1400 at 175°C.

The last sensitivity analysis, for the H_2 adsorption rate on Pt, is shown in Fig. 8. Decreasing the adsorption rate of H_2 onto Pt by four orders of magnitude, and increasing it by one order of magnitude had absolutely no effect on the ITR simulation (Fig. 8a) or on the TPR simulation (Fig. 8b) of the noncalcined samples. For the 500°C calcined samples, no effect was observed until the H_2 adsorption rate was decreased by three orders of magnitude for the ITR simulation, and no effect was seen at all for the TPR simulation even after reducing the rate by four orders of magnitude. The effect is visible at the high-temperature calcined

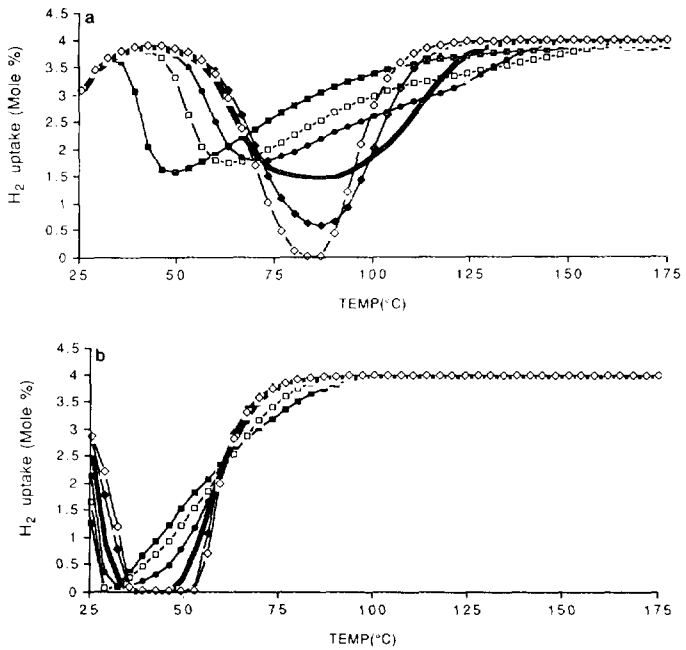

FIG. 7. (a) Effect of variation of k_{spo} and E_{sp} on TPR model for noncalcined 1% Pt/MoO_3, (k_{spo}, mol^{-1} s^{-1}/E_{sp}, cal/mol) of: —■— $4.4 \times 10^{10}/1.2 \times 10^4$; —□— $5.0 \times 10^{15}/1.8 \times 10^4$; —●— $5.4 \times 10^{17}/2.1 \times 10^4$; ▬▬ 3.7×10^{20} (BF)/2.52×10^4 (BF); —◆— $1.4 \times 10^{23}/2.9 \times 10^4$; —◇— $1.5 \times 10^{24}/3.2 \times 10^4$. (b) 500°C Calcined 1% Pt/MoO_3, (k_{spo}, mol^{-1} s^{-1}/E_{sp}, cal/mol) of: —■— $5.8 \times 10^{13}/1.0 \times 10^4$; —□— $3.0 \times 10^{16}/1.4 \times 10^4$; —●— $7.1 \times 10^{19}/1.9 \times 10^4$; ▬▬ 7.9×10^{22} (BF)/2.35×10^4 (BF); —◆— $4.2 \times 10^{26}/2.9 \times 10^4$; —◇— $4.5 \times 10^{28}/3.2 \times 10^4$.

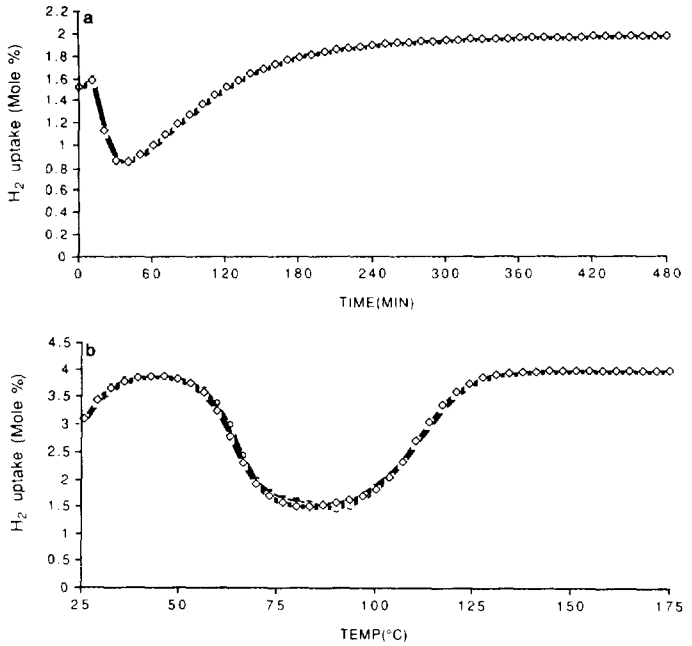

FIG. 8. (a) Effect of variation of hydrogen sticking coefficient on Pt (Sc_1) on ITR model for noncalcined 1% Pt/MoO_3, Sc_1 of: —■— 1.0×10^{-5}; —□— 1.0×10^{-4}; —●— 1.0×10^{-3}; —○— 9.9×10^{-3}; ▬▬ 9.9×10^{-2} (BF); —◇— 1.0. Noncalcined 1% Pt/MoO_3, Sc_1 of: —■— 1.0×10^{-5}; —□— 2.0×10^{-4}; —●— 1.0×10^{-3}; —○— 1.0×10^{-2}; ▬▬ 9.9×10^{-2} (BF); —◇— 1.0.

cases, since the amount of free Pt surface area is relatively very low in this case. Even so, according to the assumed model inhibition due to H_2 adsorption does not occur anywhere close to the realm of experimental conditions. The same results as those in Fig. 8 were achieved by varying the activation energy of H_2 desorption from Pt. The main conclusion here is that the adsorption equilibrium constant for H_2 adsorption onto Pt is so large that even reducing its value by three or four orders of magnitude has little effect of H_2 surface coverage of Pt.

The remainder of the modelling results of the ITR and TPR runs of Figs. 2 and 3 are plotted in Figs. 9 and 10. The surface coverage of Pt by hydrogen is shown in Fig. 9a and the MoO_3 surface coverage by hydrogen in Fig. 9b, while the amount of H in bulk MoO3 is shown in Fig. 9c, as functions of calcination temperature for the ITR simulations. The corresponding plots for $H \cdot S_0$, $H \cdot S_1$, and $H \cdot S_2$ for the TPR runs are shown in Figs. 10a, 10b, and 10c. Because the initial gas phase concentration in the TPR experiments is higher, and because the hydrogen uptake rate at the lower starting temperature of the TPR runs is lower, the Pt surface coverage during TPR runs (Fig. 10a) is always saturated with H_2, while for the ITR runs it is not. Hydrogen coverage on the MoO_3 surface shows the same trends in both simulations; slower spillover rates result in slower reduction of the MoO_3 surface. Finally, Figs. 9c and 10c represent H_2 absorption into the MoO_3 lattice, deconvoluted from the reactor effects. Differences in the initial rates of H_2 uptake as a function of calcination temperature are best seen in the simulation of the TPR experiments, Fig. 10c.

DISCUSSION

The partial corroboration of these modelling results with those of Fripiat and coworkers (*9*, *16*) is interesting, as their work

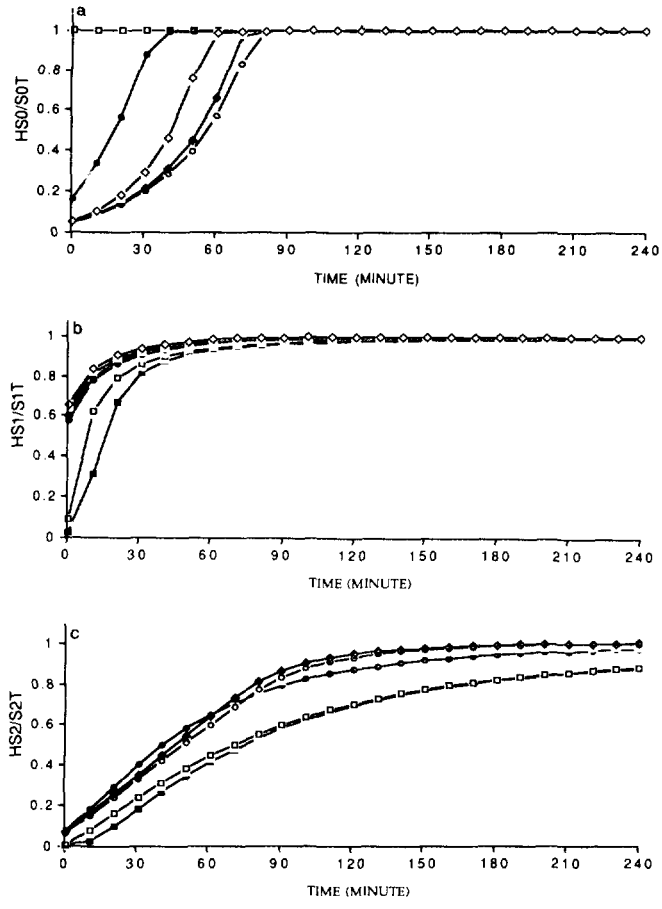

FIG. 9. (a) $H \cdot S_0$, (b) $H \cdot S_1$, and (c) $H \cdot S_2$ for ITR simulation: —■— noncalcined, calcination at: —□— 100°C, 1 hr; —●— 200°C, 1 hr; —○— 300°C, 1 h; —◆— 400°C; 1 h; —◇— 500°C, 1 h.

was conducted using a single crystal of MoO_3 at low pressure ($<5 \times 10^{-6}$ Torr). The reduction mechanism for the noncalcined and low temperature calcined samples appears to match their observations: first an induction period in which the MoO_3 surface became reduced by spillover and then a rate-determining step of H_2 adsorption directly onto the partially reduced MoO_3 surface. The two sets of results differ in that direct adsorption onto the bronze was reported as the rate-determining step for all of the single-crystal runs (*9*), that is, bulk reduction from spillover was always relatively slow. In the present study with Pt impregnated onto powdered MoO_3, spillover became faster than adsorption onto the bronze for the high-temperature calcined samples. The effect of calcination was not studied in the single crystal work (*9*, *16*), but was noted by the same group in studies of H_2PtCl_6-impregnated MoO_3 powders (*19*).

The physical factors which could be responsible for the differences in H_2 uptake caused by calcination of Pt/MoO_3 and which are consistent with the simulation results of the assumed model can now be discussed. A number of effects were addressed qualitatively in the previous work (*1*). Two, Pt crystallite size and the presence of water, were dismissed and are not considered further in the present work. The remaining two

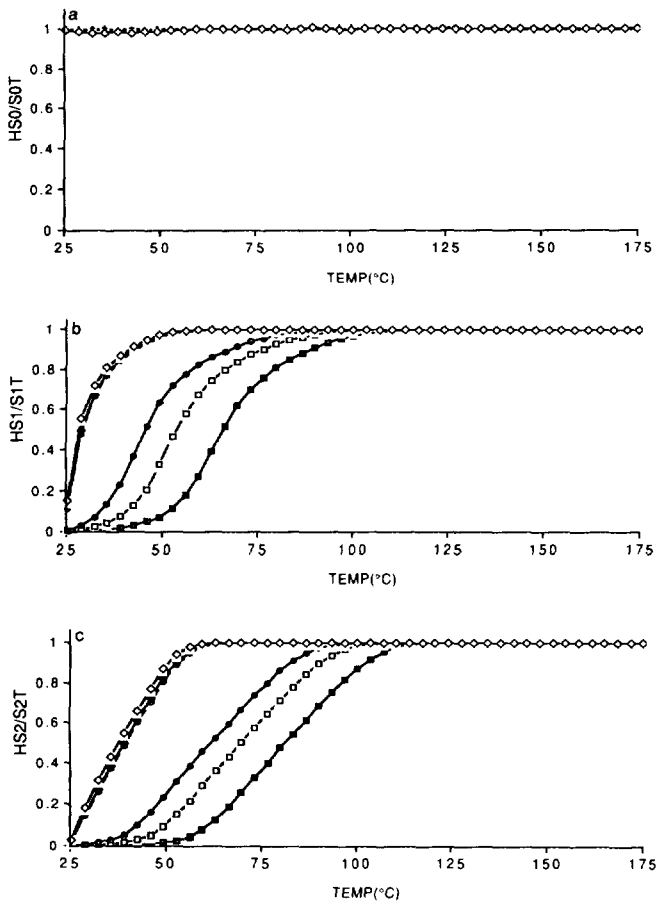

FIG. 10. (a) $H \cdot S_0$, (b) $H \cdot S_1$, and (c) $H \cdot S_2$ for ITR simulation: —■— noncalcined, calcination at: —⊟— 100°C, 1 hr; —●— 200°C, 1 hr; —○— 300°C, 1 h; —◆— 400°C; 1 h; —◇— 500°C, 1 h.

possible factors which could explain the increase of hydrogen uptake with increased calcination temperature are the growth of MoO_3 overlayers or the riddance of chlorine (*1*). The nature of these effects can be clarified somewhat.

It is first noted that the simulation is quite insensitive to the adsorption rate of H_2 on Pt (Fig. 7) and the H_2 desorption activation energy from Pt. That is, the supply of H_2 to the Pt surface is much more rapid than the amount of H_2 shuttled off of the Pt surface to MoO_3 via spillover, even for the 500°C sample, which had the highest spillover rate and the lowest amount of exposed Pt sites. Thus a possible effect of chlorine in blocking H_2 adsorption sites (*20–22*) can be discounted. The extent of site blockage has been reported to be about 50% in the case of Ru/SiO_2 (*21*). The simulation shows that a far greater extent of blockage is needed to affect the supply of hydrogen from the gas phase. Site blockage in these systems is seen only when MoO_3 overlayers are grown so extensively (at 500°C, for long calcination times) that all of the Pt sites are covered and no CO chemisorption or H_2 uptake is observed (*1*).

Perhaps the most significant manifestation of the enhanced H_2 uptake in calcined samples is seen in the way the spillover rate changes with increasing calcination temper-

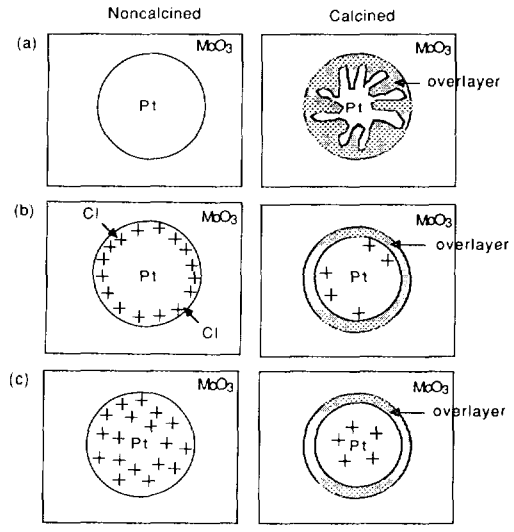

FIG. 11. Schematic of possible calcination effects: (a) MoO_3 overlayer promotion, (b) lessening of chlorine inhibition at adlineation, and (c) lessening of chlorine hindrance of H surface diffusion.

ature. According to the (admittedly rough) adjustment of fitted parameters for the TPR simulations, the activation energy for spillover decreased by slightly less than 10%, the frequency factor increases by a factor of 212 (Table 2). Several physical factors can account for this change. The first cause would be an increase in the adlineation length, or the line of contact between Pt and MoO_3. There are two ways in which this can occur. One is that MoO_3 overlayers serve to increase the adlineation length. This would occur even as the total exposed Pt area is being decreased. The physical implication to account for increasing adlineation but decreasing exposed Pt area is that MoO_3 overlayers grow in some sort of a fingerlike network over the Pt surface. The number of adlineation sites would initially correspond (for the noncalcined sample) to the number of perimeter sites at Pt particles and would then increase with overlayer growth. A schematic for an increased adlineation length due to overlayers is shown in Fig. 11a.

The removal of residual chlorine from the Pt–MoO_3 adlineation is a second manner in which the number of adlineation sites would increase as a function of calcination temperature. This interpretation is schematized in Fig. 11b. In contrast to the overlayer interpretation, the number of adlineation sites in the noncalcined, chlorine-laden samples would be much less than the number of Pt perimeter sites and would increase as the amount of chlorine decreased. In this way the chlorine effect can be thought of as a lessening of inhibition, while the overlayer effect would be considered true promotion of H_2 spillover.

Residual chlorine might also inhibit spillover in a different way: by slowing the diffusion of adsorbed hydrogen across the Pt surface to the adlineation sites. This process is also lumped into the spillover rate constant. It is sketched in Fig. 11c.

It is not possible to ascertain between these factors from the limited resolution of TEM characterization reported earlier (*1*). On the basis of control ITR experiments which isolated the effects of overlayers (Fig. 11 of (*1*)) and chlorine (Fig. 12 of (*1*)), overlayers were postulated to increase the degree of contract between Pt and MoO_3, resulting in a larger total uptake upon calcination of poorly contacted Pt + MoO_3 physical mixtures. However, the intrinsic rate of spillover from the Pt surface to the MoO_3 bulk, was shown to most strongly correlate with the amount of chlorine removed from the Pt surface. In a series of samples with the same initial dispersion of Pt precursors on MoO_3, the chlorine effect was thought to dominate the H_2 uptake spectra. Given the high insensitivity to the amount Pt surface and the rate of H_2 adsorption onto Pt in the model, however, it would not appear that H_2 needs to be supplied from large distances away from the adlineation. Blocking of the adlineation is perhaps the more reasonable of the chlorine effects.

CONCLUSIONS

A simplified intrinsic kinetics model of hydrogen spillover has been used to simulate two series of ITR and TPR experiments in Pt/MoO_3 samples, with adjustment of

only the hydrogen spillover rate constant (including the preexponential factor and activation energy in the TPR simulations) and the rate constant for H_2 adsorption onto a partially reduced MoO_3 surface, and H_2 back penetration for the noncalcined samples.

A mechanistic interpretation of the experimental results of hydrogen bronze formation in a series of calcined Pt/MoO_3 samples, consistent with the assumed mechanism is as follows:

(1) for the noncalcined or low-temperature (100°C) calcined samples, formation of the hydrogen bronze occurs by a series–parallel mechanism: first, reduction of the MoO_3 surface by hydrogen spillover from Pt must occur, but then direct adsorption of H_2 onto the partially reduced MoO_3 surface supplies most of the hydrogen to the MoO_3 bulk.

(2) In the high-temperature calcined samples, the rate of hydrogen spillover increases by three orders of magnitude with respect to the noncalcined sample such that spillover is the single rate-determining step.

(3) In the high-temperature calcined simulations, the activation energy for spillover decreases a small amount, while the preexponential factor increases up to 212 times. This trend could arise from an increased number of adlineation sites due to a promotional effect of MoO_3 overlayers; however, from a comparison with earlier experimental characterization, the more plausible explanation for this trend is a lessening of blockage of adlineation sites or hindrance of hydrogen diffusion across the Pt surface by chlorine.

(4) Blockage of H_2 adsorption on Pt by chlorine does not appear to play a factor in the observed kinetics.

APPENDIX: NOMENCLATURE

k_1 = H_2 adsorption rate constant onto S_0 (s^{-1}) = $k_{col1} \times Sc_1$
k_2 = H_2 desorption rate from S_0 ($mol^{-1}\ s^{-1}$)
k_{sp} = H_2 spillover rate ($mol^{-1}\ s^{-1}$) = $k_{spo}\exp(-E_{sp}/RT)$
k_{spo} = H_2 spillover rate preexponential ($mol^{-1}\ s^{-1}$)
k_4 = H_2 spillover rate ($mol^{-1}\ sec^{-1}$) = $k_{40}\exp(-E_4/RT)$
k_5 = H_2 back diffusion rate ($mol^{-1}\ s^{-1}$) = $k_{50}\exp(-E_5/RT)$
k_6 = H_2 adsorption rate onto S_1 (s^{-1}) = $k_{col6} \times Sc_6$
E_2 = H_2 desorption activation energy from S_0 (cal/mol)
E_{sp} = H_2 spillover activation energy (cal/mol)
E_4 = H_2 penetration activation energy (cal/mol)
E_5 = H_2 back diffusion activation energy (cal/mol)
E_6 = H_2 desorption activation energy (cal/mol)
S_0 = number of Pt sites (mol)
S_1 = number of surface MoO_3 sites (mol)
S_2 = number of bulk MoO_3 sites (mol)
$H \cdot S_0$ = number of moles occupied by H on site 0 (Pt)
$H \cdot S_1$ = number of moles occupied by H on site 1 (MoO_3 surface)
$H \cdot S_2$ = number of moles occupied by H on site 2 (MoO_3 bulk)
θ_{S0} = mole fraction of H on site 0
θ_{S1} = mole fraction of H on site 1
Sc_1 = sticking coefficient for H_2 on Pt
Sc_2 = sticking coefficient for H_2 on MoO_3
H_{2in} = H_2 concentration of reactor inlet (mol/cm^3)
H_2 = H_2 gas phase concentration
Q = flow rate (cm^3/min)
V = volume of reactor (cm^3)

ACKNOWLEDGMENTS

Research support from the Amoco Corporation and the Illinois Department of Commerce and Community Affairs (DCCA) is gratefully acknowledged.

REFERENCES

1. Kim, J.-G., Shyu, J., and Regalbuto, J. R., *J. Catal.* **139,** 153 (1993).
2. Herz, R. K., and Marin, A. P., *J. Catal.* **65,** 281 (1980).
3. Kaul, D. J., Sant, R. and Wolf, E. E., *Chem. Eng. Sci.* **42**(6), 1399 (1987).
4. Davenport, J. W., and Dienes, G. J., *Phys. Rev.* **25**(4), 2165 (1982).
5. Leary, K. J., Michaels, J. N., and Stacy, A. M., *AIChE J.* **34** (2), 263 (1988).
6. Leary, K. J., Michaels, J. N., and Stacy, A. M., *Langmuir* **4,** 1251 (1988).
7. Klein, R. L., and Schmidt, L. D., *J. Chem. Phys.* **76**(7), 3824 (1982).
8. Taylor, R. E., Silva Crawford, M. M., and Gerstein, B. C., *J. Catal.* **62,** 401 (1980).
9. Erre, R., Legay, M. H., and Fripiat, J. J., *Surf. Sci.* **127,** 69 (1983).
10. Thomas, R., and Moulijn, J. A., *J. Catal.* **84,** 257 (1983).
11. Seebauer, E. G., Kong, A. C. F., and Schmidt, L. D., *Surf. Sci.* **176,** 134 (1986).
12. Zhdanov, V. P., *Surf. Sci.* **169,** 1 (1986).
13. Nishiyama, Y., and Wise, H., *J. Catal.* **32,** 50 (1974).
14. Cirillo, A., and Fripiat, J. J., *J. Phys.* **39,** 247 (1978).
15. Christmann, K., Ertl, G., and Pignet, T., *Surf. Sci.* **54,** 365 (1976).
16. Erre, R., Van Damme, H., and Fripiat, J. J., *Surf. Sci.* **127,** 48 (1983).
17. Lin, X., Francois, J., Lambert, H., and Fripiat, J. J., *Catal. Lett.* **3,** 169 (1989).
18. Datta, A., Ha, J.-W., and Regalbuto, J. R., *J. Catal.* **133,** 55 (1992).
19. Tinet, D., and Fripiat, J. J., *J. Chim. Phys. Phys. Chim. Biol.* **76,** 867 (1979).
20. Bond, G. C., and Rajaram, R. R., *Appl. Catal.* **27,** 379 (1986).
21. Narita, T., Miura, H., Sugiyama, K., Matsuda, T., and Gonzalez, R. D., *J. Catal.* **103,** 492 (1987).
22. Tiep, L. V., Che, M., Bugli, G., and Bond, G. C., *J. Catal.* **99,** 449 (1986).